2008

Air-Side Heat Transfer and Pressure Drop in Accelerated Flow Evaporators

Paulo J. Waltrich
Federal University of Santa Catarina

Jader R. Barbosa
Federal University of Santa Catarina

Claudio Melo
Federal University of Santa Catarina

Christian J. L. Hermes
Federal University of Santa Catarina

Rodrigo Kremer
Whirlpool Corporation

Air-Side Heat Transfer and Pressure Drop in Accelerated Flow Evaporators

Paulo J. WALTRICH, Jader R. BARBOSA Jr.*, Cláudio MELO, Christian J. L. HERMES

Federal University of Santa Catarina, Department of Mechanical Engineering,
Florianópolis, SC, 88040900, Brazil

* Corresponding Author
Phone/Fax: ++ 55 48 3234 5166, e-mail: jrb@polo.ufsc.br

ABSTRACT

The performance of an alternative evaporator design for household applications, the so-called Accelerated Flow Evaporator (AFE), is investigated in this paper. In this novel concept, the air-side cross sectional area decreases with the distance from the air flow inlet, accelerating the air as it flows across the tubes and, therefore, improving the air-side local heat transfer coefficient. In principle, some geometrical configurations of the AFE are expected in which the heat transfer coefficient enhancement compensates the reduction of the heat exchanger surface for a given refrigeration capacity, thus reducing the material cost of the evaporator. Experiments have been conducted in an open-loop wind tunnel facility to determine the air-side heat transfer and pressure drop in nine AFE prototypes as a function of the air flow rate, the ratio of the outlet and inlet cross-section area and the number of fins. A calculation methodology has been proposed to correlate the air-side heat transfer and pressure drop in the AFE. The procedure relies on *j* and *f* factor correlations for plain fin-and-tube heat exchanger surfaces and on mass and momentum balances to determine the by-pass air stream through the clearance between the tube bank and the outer edge of the fins. The agreement between the model and the experiments is within ±10% for all heat transfer data and ±15% for the majority of the pressure drop data.

1. INTRODUCTION

There are more than one billion domestic refrigerators currently in operation worldwide (Coulomb, 2006) and the so-called 'no-frost' (or 'frost-free') refrigerators represent a substantial and increasing fraction of this number. In 'no-frost' refrigerators, compartment cooling relies on forced convection heat transfer between the internal air (assisted by a fan) and a tube-fin evaporator. The evaporator has an important role in the determination of the system performance because it is responsible for providing the cooling capacity required for preserving the goods stored in the refrigerator at the desired temperatures. Hence, improving the performance of the evaporator is potentially significant as a means of improving the performance of the whole system and, consequently, as a means of promoting material cost savings.

Cur and Anselmino (1992) proposed an alternative configuration of a tube-fin evaporator for 'no-frost' domestic appliances, the so-called *Accelerated Flow Evaporator* (AFE). The main purpose of this concept is to reduce the size of the evaporator (and hence the volume of aluminum) by enhancing the local air-side heat transfer coefficient. This local intensification is achieved through a progressive reduction of the air-side cross-sectional area, which results in an increase of the mean velocity of the air stream and hence the local Reynolds number (see Fig. 1). The main drawback of the AFE configuration is an intrinsic increase of the reversible and irreversible components of the air-side pressure drop of the evaporator.

So far, there has been no systematic study of this type of evaporator in the open literature and the real benefits of its volumetric reduction and associated increase in air-side pressure drop in comparison with the standard 'no-frost' evaporator are yet to be fully quantified. Even for conventional 'no-frost' evaporators, there is a dearth in the open literature regarding systematic studies of their thermal-hydraulic performance. The reader is referred to the paper of

Barbosa *et al.* (2008) for an appraisal of the recent studies on the air-side heat transfer and pressure drop in 'no-frost' evaporators.

Therefore, the objective of this paper is to present a systematic study of the influence of two geometric parameters (number of fins and outlet height) and of the air flow rate on the air-side thermal-hydraulic performance of a AFEs under 'dry' conditions (no condensate or frost formation). The experimental work is complemented by a calculation methodology to correlate the heat transfer and pressure drop on the air-side.

2. EXPERIMENTAL WORK

2.1 Evaporator Samples

Nine evaporator samples made from copper (tubes) and aluminium (fins) were tested. The inner and outer diameters of the tubes in all evaporators were 7.80 and 8.80 mm, respectively. A staggered tube array was used. The fins were flat, plain and continuous. The refrigerant circuitry was designed to provide a full counter-flow heat exchanger configuration. Figure 1 shows a side view of the evaporator samples illustrating the cross-sectional area reduction in the direction of the flow. The width W, the inlet height (thickness) H_{in} and the fin thickness in all samples are 310 mm, 192 mm and 0.25 mm, respectively. The evaporator outlet height (H_{out}), number of fins, the total surface area of fins and tubes, the fin spacing and the amount of material (evaporator mass) are different for each individual sample and their values are summarized in Tab. 1.

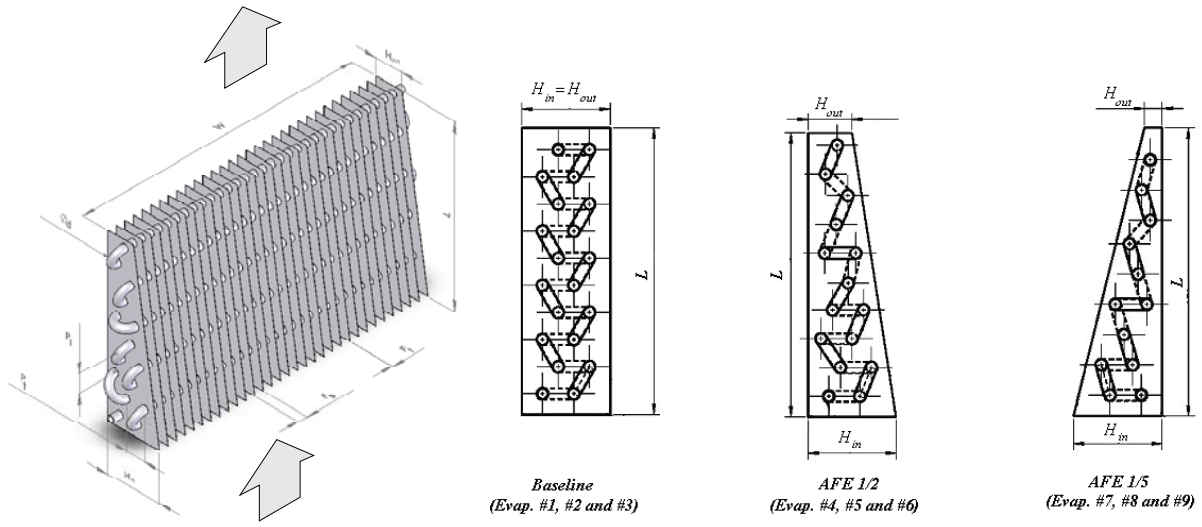

Figure 1. Geometry of the AFE and design of the evaporator samples.

Table 1: Geometric parameters of evaporator samples.

Evaporator	H_{out} (mm)	Number of fins	Number of tubes	Area (m^2)	Fin pitch (mm)	Mass (kg)
#1	59.5	60	20	1.40	5.15	1.242
#2	59.5	30	20	0.78	10.30	1.030
#3	59.5	2*	20	0.16	310	0.823
#4	29.75	60	15	1.05	5.15	0.884
#5	29.75	30	15	0.61	10.30	0.843
#6	29.75	2*	15	0.17	310	0.585
#7	11.9	57	12	0.83	5.50	0.734
#8	11.9	30	12	0.48	10.30	0.643
#9	11.9	2*	12	0.12	310	0.522

* Structural fins placed adjacent to the tube bends.

2.2. Experimental Apparatus and Procedure

The experimental apparatus and the test procedure are identical to that reported in Barbosa *et al.* (2008). The evaporator samples presented in Tab. 1 were tested at five different air flow rates equally distributed between 34 ± 1 and 102 ± 2 m^3/h. The inlet air temperature was varied between 20.5 ± 0.2 and 28.1 ± 0.2 °C and the average water temperature was kept constant at 36 ± 0.1°C. In total, 60 experimental data points have been collected, including the repeatability assessment measurements.

3. DATA REGRESSION

The overall thermal conductance was calculated using the Log-Mean Temperature Difference approach (Lienhard and Lienhard, 2005), as follows

$$UA = \frac{\dot{Q}_a}{(F\Delta T_{lm})} = \frac{\dot{Q}_a \ln[(T_w - T_{a,i})/(T_w - T_{a,o})]}{(T_w - T_{a,i}) - (T_w - T_{a,o})} \tag{1}$$

where F has been assumed equal to unity as the water flow rate through the coils was adjusted so that its thermal capacity was much larger than that of the air stream (temperature drop of the order of 0.5°C between the water inlet and outlet). According to the recommendations of the ASHRAE 37 (1988), the difference between the thermal capacities measured on the water and air sides was lower than 5% in all experimental runs. The uncertainty levels corresponding to the pressure drop, heat transfer capacity (air-side), and overall thermal conductance have been estimated at ±5%, ±5% and ±7%, respectively (Waltrich, 2008).

4. MATHEMATICAL MODELING

The modeling approach consists of dividing the evaporator into n control volumes in the direction of the air flow. The tube pitches, fin density and inlet and outlet cross-sectional areas can be set independently for each control volume. The momentum and energy conservation equations are written for a generic control volume and are integrated along the evaporator to obtain the air-side pressure drop and heat transfer capacity. The following assumptions have been adopted in the model: (i) steady-state; (ii) negligible body forces; (iii) constant tube wall temperature in each control volume; (iv) heat transfer and friction coefficients uniform in each control volume; (v) dry air is modeled as an ideal gas; and (vi) incompressible flow with constant properties in each control volume.

An important feature of the present model is that it takes into account that part of the air flow by-passes the tubes through the side clearances (or gaps), as shown in Fig. 2. In typical 'no-frost' evaporators, the by-pass air flow rate may become significant, as the flow resistance along the gap is usually of the same order of magnitude as the resistance associated with the flow across the tube array. Barbosa *et al.* (2006) reported that at least 40% of the total air flow rate by-passes the tube array through the side gaps in a typical 'no-frost' evaporator with the defrosting heater coils mounted on. Obviously, this reduction of the air flow rate across the tubes decreases the heat exchanger effectiveness and should be avoided in the evaporator design. The air-side resistance circuitries are shown in Fig. 2.

The air-side pressure drop in an AFE is given by

$$\Delta p_{AFE} = \Delta p_{i-o} = \Delta p_{i-i'} + \Delta p_{i'-o'} + \Delta p_{o'-o} \tag{2}$$

where $\Delta p_{i-i'}$, $\Delta p_{i'-o'}$ and $\Delta p_{o'-o}$ are the pressure changes associated with the inlet contraction, the tube array and side gaps, and the outlet expansion, respectively. In terms of the concept of flow resistance, one can write

$$\Delta p_{i-i'} = R_{\Delta P,in}\dot{m}_a = \left(\frac{K_c \dot{m}_a}{2A_{i'}^2 \rho_a}\right)\dot{m}_a \tag{3}$$

$$\Delta p_{o'-o} = R_{\Delta P,out}\dot{m}_a = \left(\frac{K_e \dot{m}_a}{2A_{o'}^{\ 2}\rho_a}\right)\dot{m}_a \tag{4}$$

$$\Delta p_{i'-o'} = \sum_{k=1}^{n} {}^{k}R_{\Delta P,t}\,{}^{k}\dot{m}_{a,t} \tag{5}$$

$$\Delta p_{i'-o'} = \sum_{k=1}^{n} {}^{k}R_{\Delta P,bp}\,{}^{k}\dot{m}_{a,bp} \tag{6}$$

where *k* corresponds to a generic control volume between the inlet and outlet. Mass conservation requires that

$$\dot{m}_a = {}^{k}\dot{m}_{a,t} + 2\,{}^{k}\dot{m}_{a,bp} \tag{7}$$

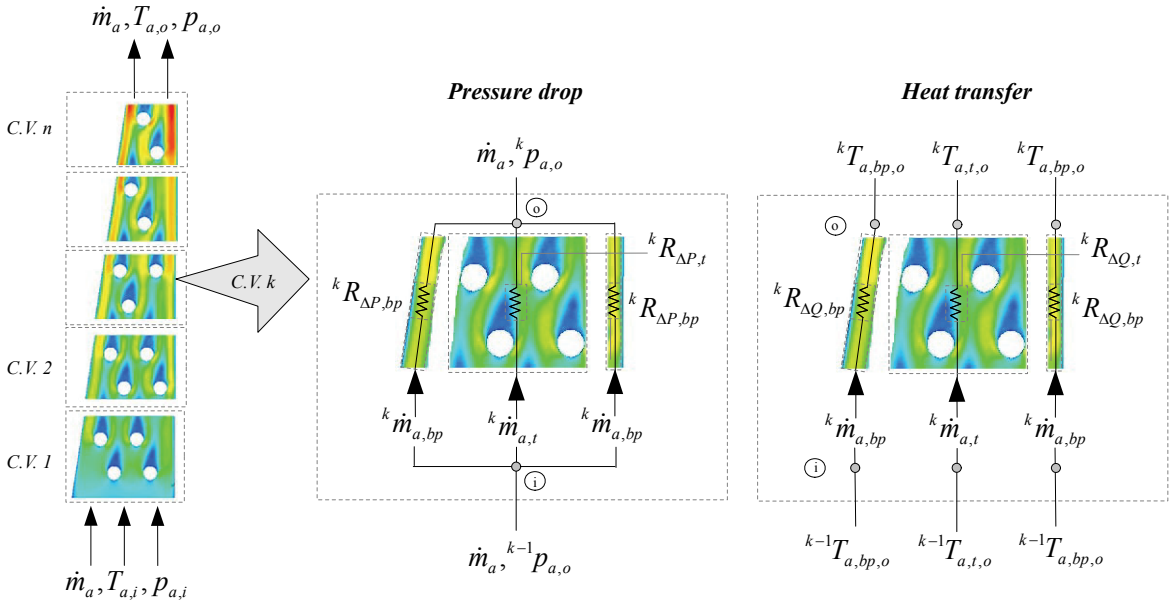

Figure 2. Description of the model.

If the resistances associated with the flow across the tubes and through the side gaps are known from the momentum balances in each control volume, then equations (3) to (7) can be solved simultaneously to give: $\Delta p_{i-i'}$, $\Delta p_{i'-o'}$, $\Delta p_{o-o'}$, $\dot{m}_{a,t}$ and $\dot{m}_{a,bp}$. After integrating the momentum balances in each control volume, the flow resistances can be written as (Waltrich, 2008)

$${}^{k}R_{\Delta P,t} = \frac{{}^{k}\tau_t\,{}^{k}A_t}{{}^{k}A_{m,t}\,{}^{k}\dot{m}_{a,t}} + \frac{{}^{k}V_{a,t}}{{}^{k}A_{m,t}}\left[\ln\left(\frac{{}^{k}T_{a,t,o}}{{}^{k}T_{a,t,i}}\right) - \ln\left(\frac{{}^{k}p_{a,o}}{{}^{k}p_{a,i}}\right)\right] + \frac{{}^{k}V_{a,t}W\tan\theta\,{}^{k}L}{{}^{k}A_{m,t}^{2}} \tag{8}$$

$${}^{k}R_{\Delta P,bp} = \frac{{}^{k}\tau_{bp}\,{}^{k}A_{bp}}{{}^{k}A_{m,bp}\,{}^{k}\dot{m}_{a,bp}} + \frac{{}^{k}V_{a,bp}}{{}^{k}A_{m,bp}}\left[\ln\left(\frac{{}^{k}T_{a,bp,o}}{{}^{k}T_{a,bp,i}}\right) - \ln\left(\frac{{}^{k}p_{a,o}}{{}^{k}p_{a,i}}\right)\right] \tag{9}$$

where the first and second terms on the right hand side of equations (8) and (9) result from friction and acceleration due to the density change along the control volume. The third term on the right hand side of equation (8) is the reversible pressure drop due to the reduction of the cross-sectional area (i.e., the Bernoulli Effect).

The air side heat transfer is given by (note that the heat transfer in the inlet contraction and outlet expansion has been neglected)

$$\dot{Q}_T = \sum_{k=1}^{n} \left({}^{k}\dot{Q}_t + 2\,{}^{k}\dot{Q}_{bp} \right) \tag{10}$$

$${}^{k}\dot{Q}_t = {}^{k}\dot{m}_{a,t} c_{pa} ({}^{k}T_{a,t,i} - {}^{k}T_{a,t,o}) \tag{11}$$

$${}^{k}\dot{Q}_{bp} = {}^{k}\dot{m}_{a,bp} c_{pa} ({}^{k}T_{a,bp,i} - {}^{k}T_{a,bp,o}) \tag{12}$$

and the continuity of temperatures between control volumes guarantees that ${}^{k}T_{a,t,i} = {}^{k-1}T_{a,t,o}$ and ${}^{k}T_{a,bp,i} = {}^{k-1}T_{a,bp,o}$. After integration, the energy balances for each control volume gives (Waltrich, 2008)

$$\frac{{}^{k}T_{a,t,o} - {}^{k}T_w}{{}^{k}T_{a,t,i} - {}^{k}T_w} = \exp\left(\frac{{}^{k}\eta_o \, {}^{k}h_t \, {}^{k}A_t}{{}^{k}\dot{m}_{a,t} \, {}^{k}c_{p,a}} \right) \tag{13}$$

$$\frac{{}^{k}T_{a,bp,o} - {}^{k}T_w}{{}^{k}T_{a,bp,i} - {}^{k}T_w} = \exp\left(\frac{{}^{k}\eta_f \, {}^{k}h_{bp} \, {}^{k}A_{bp}}{{}^{k}\dot{m}_{a,bp} \, {}^{k}c_{p,a}} \right) \tag{14}$$

The wall shear stresses and heat transfer coefficients have been calculated using the following closure relationships

$${}^{k}\tau_t = \frac{1}{2} \frac{{}^{k}f_t}{{}^{k}\rho_a} \left(\frac{{}^{k}\dot{m}_{a,t}}{{}^{k}A_{m,t}} \right)^2 ; \quad {}^{k}\tau_{bp} = \frac{1}{2} \frac{{}^{k}f_{bp}}{{}^{k}\rho_a} \left(\frac{{}^{k}\dot{m}_{a,bp}}{{}^{k}A_{m,bp}} \right)^2 \tag{15}$$

$${}^{k}h_t = {}^{k}j_t \left(\frac{{}^{k}\dot{m}_{a,t}}{{}^{k}A_{m,t}} \right) \frac{{}^{k}c_{p,a}}{{}^{k}\mathrm{Pr}_a^{2/3}} ; \quad {}^{k}h_{bp} = {}^{k}j_{bp} \left(\frac{{}^{k}\dot{m}_{a,bp}}{{}^{k}A_{m,bp}} \right) \frac{{}^{k}c_{p,a}}{{}^{k}\mathrm{Pr}_a^{2/3}} \tag{16}$$

where ${}^{k}f_t$ and ${}^{k}j_t$ were calculated using the correlation of Wang and Chang (1998) for tube-fin heat exchangers. ${}^{k}f_{bp}$ and ${}^{k}j_{bp}$ were calculated through correlations for the laminar flow in a boundary-layer on a flat plate (Lienhard and Lienhard, 2005). The overall surface efficiency was calculated from

$${}^{k}\eta_o = 1 - \frac{{}^{k}A_{f,t}}{{}^{k}A_t} (1 - \eta_f) \tag{17}$$

where η_f is the fin efficiency calculated using the approach of Perrotin and Clodic (2003).

4. RESULTS AND DISCUSSION

4.1. Experimental Results

Figure 3 shows the overall thermal conductance for each sample as a function of the air flow rate. None of the AFE samples performed better in terms of *UA* than their baseline counterparts, which is an indication that the amount of surface area is the most important factor in determining the magnitude of *UA*. Figure 4 presents the experimental results in terms of the overall heat transfer coefficient *U*, calculated as the ratio of the overall thermal conductance and the external heat transfer surface. The heat transfer coefficient is higher for the evaporators with no fins and decreases with increasing surface area. It is hypothesized that this is because the fins break-up the large three-dimensional flow structures which contribute to an increase of the momentum and heat transfer in the transverse

direction. For a fixed value of the fin pitch, the AFE samples show higher values of the heat transfer coefficient, which is a demonstration of the enhancement associated with the Bernoulli Effect. For the lowest values of the fin pitch (samples #1, #4 and #7), however, this enhancement is not very clear. As will be shown later, this may be due to the influence of the fraction of the air stream which by-passes the tube bank through the side clearances.

Figure 5 shows the pressure drop as a function of the air flow rate. All AFE samples have pressure drops greater that their respective baseline counterparts due to the velocity increase associated with the Bernoulli Effect. The values of pressure drop shown in Fig. 5 take into account only the frictional component, as the reversible (acceleration induced) component can be deducted from the measured pressure gradient as follows (Waltrich, 2008)

$$\Delta p_F = (p_i - p_o) - \frac{\dot{m}_a^{\,2} \tan\theta}{\rho W^2} \frac{L(2H_1 - \tan\theta L)}{2H_1^{\,2}(H_1 - \tan\theta L)^2} \tag{20}$$

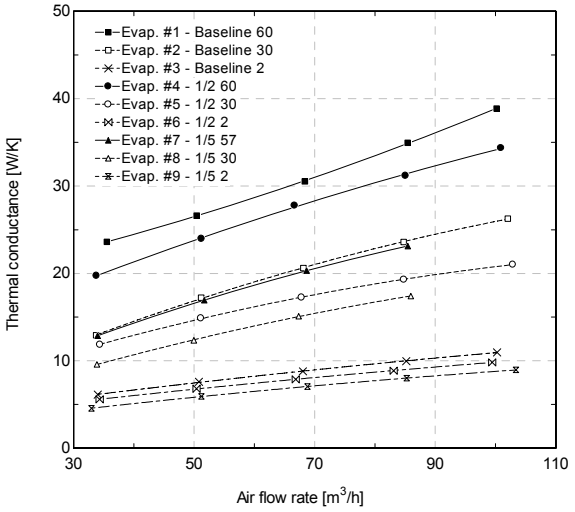

Figure 3. Thermal conductance.

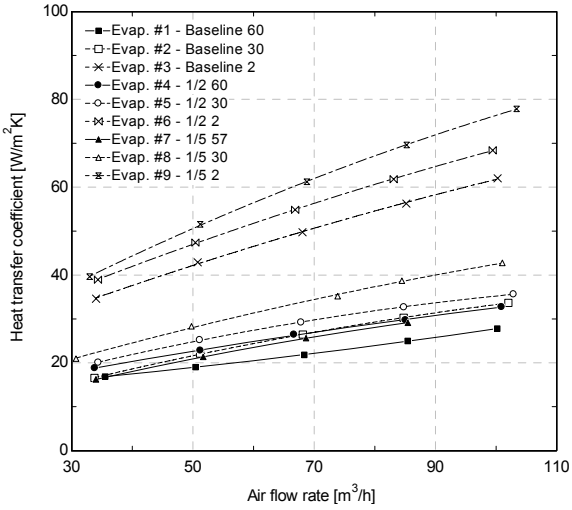

Figure 4. Heat transfer coefficient.

As can be seen from Fig. 5, sample #9 has a greater pressure drop than sample #8 in spite of the larger number of fins in the latter (both are 1/5 AFEs). Again, it is hypothesized that this is due to the fact that the fins inhibit the formation of large secondary flow structures that would otherwise appear as a result of the change in flow direction experienced in the 1/5 AFEs.

4.2. Model Results

The model has been used to calculate the heat transfer capacity and the total pressure drop of each evaporator sample. The overall performance of the model is shown in Figs. 6 and 7. The heat transfer results agree with the data to within ±10% and the pressure drop can be predicted to within ±15%, except for sample #4. The level of agreement can be considered satisfactory given that no fitting parameters have been used to adjust independent correlations to the present data.

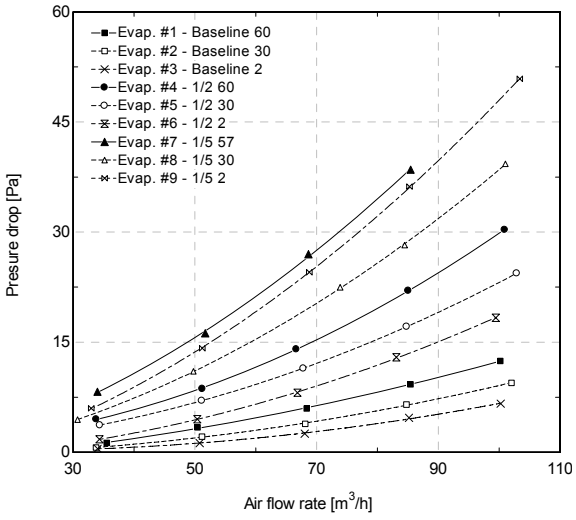

Figure 5. Pressure Drop.

As mentioned above, the fraction of the total air flow rate through the side gaps (clearance by-pass) can be significant in the AFEs and in 'no-frost' evaporators in general. The by-pass fractions, defined as the ratio of the mass flow rate through the by-pass and the total mass flow rate, calculated for each evaporator are shown in Fig. 8

as a function of the total air flow rate. The by-pass fraction associated with the 1/5 AFE is the largest, which may explain its lower heat transfer coefficient in comparison to sample #4. The by-pass fractions of evaporators #1 and #2 are larger than the 1/2 AFE samples possibly because the width of the clearance channels is larger in the baseline prototypes (8 mm) than in the 1/2 AFE samples (4.5 mm).

Figure 9 presents a comparative evaluation of the performance of the AFE concept. The pumping power as a function of the heat transfer capacity as calculated from the mathematical model is plotted for each evaporator sample. At low heat transfer capacities, the performances of all evaporators are quite similar as a small pumping power is required for a specified capacity. Thus, under such conditions, the AFE concept may be more advantageous than the baseline (straight) evaporators because of its lower material costs. At high heat transfer capacities, however, the pumping power of the AFEs increases exponentially (because of the lower heat transfer surface area), thus undermining its energetic performance.

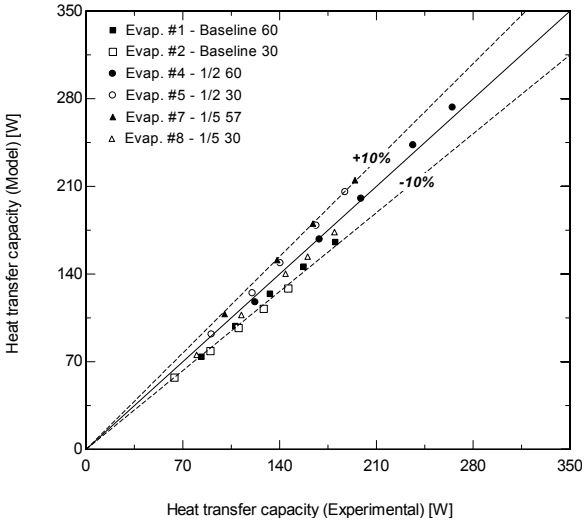

Figure 6. Heat transfer capacity prediction.

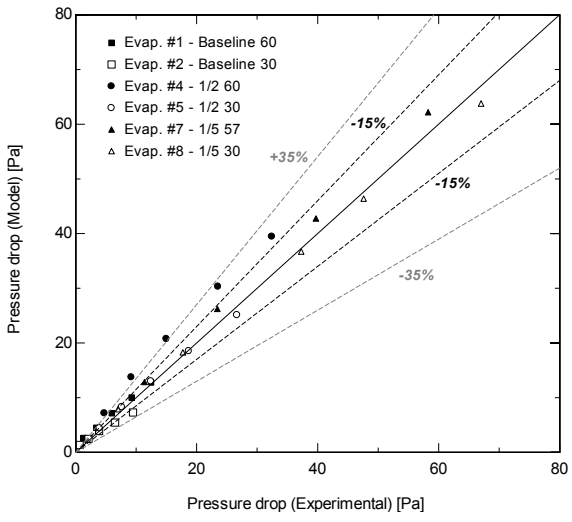

Figure 7. Pressure drop prediction.

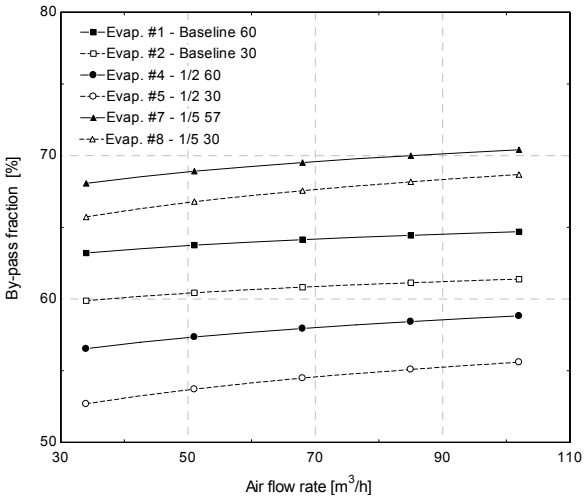

Figure 8. By-pass fraction as a function of flow rate.

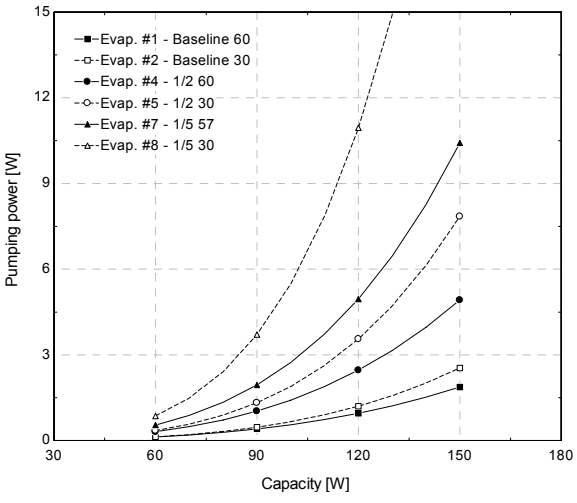

Figure 9. Pumping power as a function of capacity.

5. CONCLUSIONS

This paper presented experimental data on an alternative concept for a 'no-frost' household refrigeration evaporator. In this novel concept, the air-side cross-sectional area decreases with distance from the inlet, accelerates the flow and promotes an enhancement of the local heat transfer coefficient. Nine prototypes have been tested in a purpose-

built experimental facility. A model has been proposed for calculating the heat transfer capacity and pressure drop in the AFE taking into account the by-pass flow rate through the side gaps. The model, which possesses no fitting parameters, predicted the experimental heat transfer capacity and pressure drop data to within ±10% and ±15%, respectively. The study showed that for low heat transfer capacities, the performances of the baseline and accelerated flow evaporators are quite similar as a small pumping power is required for a specified capacity. Thus, under such conditions, the AFE concept may be more advantageous than the straight evaporators because of its lower material costs. At high heat transfer capacities, however, the pumping power of the AFEs increases exponentially, thus preventing it from being energetically viable.

NOMENCLATURE

A	area	(m^2)	**Subscripts**	
c_P	specific heat capacity	(J/kg.K)	a	air
F	correction factor	(-)	bp	by-pass
H	evaporator height	(m)	c	contraction
h	heat transfer coefficient	($W/m^2.K$)	e	expansion
K	pressure drop factor	(-)	f	fin
k	generic control volume	(-)	i	inlet
L	evaporator length	(m)	m	minimum flow passage
$\dot{m}$	mass flow rate	(kg/s)	N	evaporator sample
p	pressure	(Pa)	o	outlet
Pr	Prandtl number	(m)	t	tube array
$\dot{Q}$	heat transfer rate	(W)	w	water
R	flow resistance	($m^{-1}s^{-1}$)		
T	temperature	(^oC)	**Greek symbols**	
UA	overall thermal conductance	(W/K)	η	efficiency
V	velocity	(m/s)	ρ	density
			τ	wall shear stress
			θ	AFE angle

REFERENCES

ANSI/ASHRAE 37, 1988, Methods of Testing for Rating Unitary Air-Conditioning and Heat Pump Equipment, Atlanta-GA, USA

Barbosa Jr., J.R., Dubiela, G.A., Waltrich, P.J., 2006, Experimental, Theoretical and Numerical Analysis of Air-Side Heat Transfer and Fluid Flow in Tube-Fin Heat Exchangers, *Internal Report,* Federal University of Santa Catarina, Florianopolis-SC, Brazil (in Portuguese).

Barbosa Jr., J.R., Melo, C., Hermes, C.J.L., 2008, A Study of the Air-Side Heat Transfer and Pressure Drop Characteristics of Tube-Fin 'No-Frost' Evaporators, *Proc.12th Int. Refrigeration and Air Conditioning Conference at Purdue*, West Lafayette-IN, USA, Paper 2310

Coulomb, D., 2006, Refrigeration: The Challenges Associated with Sustainable Development, *Proc. 6th Int. Conference on Compressors and Coolants,* Slovak Republic, CD-ROM

Cur, N. O., Anselmino, J. J., 1992, Evaporator for Home Refrigerator, *US Patent* 5,157,941

Lienhard, J.H., Lienhard, J.H., 2005, *A Heat Transfer Textbook*, 3rd edition, Phlogiston Press, Cambridge-MA, USA

Perrotin, T., Clodic, D., 2003, Fin Efficiency Calculation in Enhanced Fin-and-Tube Heat Exchangers in Dry Conditions, 20th *International Congress of Refrigeration*, Washington-DC, USA

Waltrich, P.J., 2008, Analysis and Optimization of Accelerated Flow Evaporators for Household Refrigeration Applications, MSME thesis, Federal University of Santa Catarina, Florianopolis-SC, Brazil (in Portuguese)

Wang, C.-C., Chang, C.-T., 1998, Heat and Mass Transfer for Plate Fin-and-Tube Heat Exchangers with and without Hydrophilic Coating, *Int. J. Heat Mass Transfer*, 41, 3109-3120

ACKNOWLEDGEMENTS

The authors are grateful to Messrs. J. Boeng and I. Machado for their valuable support in the experimental work. Financial support from Whirlpool S.A. and the Brazilian funding agencies FINEP and CNPq is duly acknowledged.